Experiments in Fluids (2023) 64:25
https://doi.org/10.1007/s00348-022-03565-9

RESEARCH ARTICLE

Characterizing porous disk wakes in different turbulent inflow conditions with higher-order statistics

Magnus K. Vinnes[1] · Ingrid Neunaber[1] · Hauk-Morten H. Lykke[1,2] · R. Jason Hearst[1]

Received: 29 July 2022 / Revised: 15 December 2022 / Accepted: 23 December 2022

Abstract

The wakes of a uniform and a non-uniform porous disk exposed to two different turbulent flows are investigated experimentally. The disks are representative of static wind turbine models found in literature. Six wake profiles were collected through hot-wire anemometry between three and 30 diameters downstream of the disks. Both one-point and two-point statistics are studied. The results show that higher freestream turbulence affects the wake of the uniform disk more than that of the non-uniform disk, also changing the wake's shape and recovery rate. Furthermore, we confirm earlier findings that the turbulence at the centerline in the developed part of the wake is independent of both the design of the wake-generating object and the inflow. Similar to findings in the wake of a wind turbine, a ring of high intermittency is found at the very edge of the wakes of both disks and in both inflow conditions. We identify the existence of this ring over a range of scales. The results show that, even for higher-order two-point statistics, the developed wake of different porous disks qualitatively agrees well with the wake of wind turbine models.

Graphical abstract

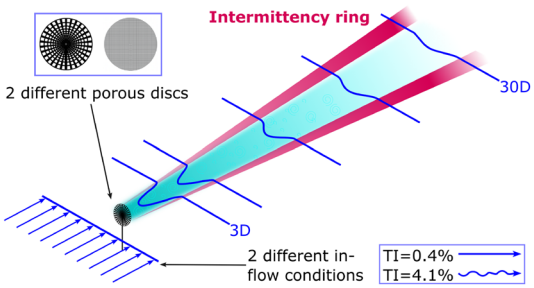

✉ R. Jason Hearst
jason.hearst@ntnu.no

Magnus K. Vinnes
magnus.kyrkjebo@ntnu.no

Ingrid Neunaber
ingrid.neunaber@ntnu.no

Hauk-Morten H. Lykke
haly@cowi.com

[1] Department of Energy and Process Engineering, Norwegian University of Science and Technology, Kolbjørn Hejes Vei 1, 7034 Trondheim, Norway

[2] Present Address: COWI AS, Stakkevollveien 41, 9010 Tromsø, Norway

1 Introduction

The description of the axisymmetric turbulent far wake is a canonical problem in fluid mechanics that has been studied extensively over the past decades (e.g., Townsend (1976) and George (1989)). An analytical solution exists for the evolution of an axisymmetric turbulent far wake of a bluff body in laminar inflow (Pope 2000). Experimentally (and numerically), wakes have classically been investigated using bluff bodies like disks exposed to laminar inflow (Hwang and Baldwin 1966; Johansson et al. 2003; Tutkun et al.

Published online: 24 January 2023

2008). In recent years, however, studies have also started to look into the impact that turbulent inflow or different types of disks have on the evolution of the wake. While some of these studies are motivated from a turbulence perspective, others have a practical motivation and build a bridge between applied problems and the initial turbulence problem. Both perspectives are discussed below.

Typically, at least two (and up to four (Brown and Roshko 2012)) different regions are distinguished in the wake, i.e., the near wake and the far wake. In the near wake, the direct interaction between the wake-generating object and the flow is visible, shear layers expand between the faster ambient flow and the slower wake, and structures such as vortices shedding from the wake-generating object are identifiable. The far wake starts where the shear layers have met, the turbulence in the wake is fully developed and the wake exhibits approximately self-similar behavior. The most prominent aspect of wake studies are the evolution of the mean velocity deficit and the wake width. Particularly, the investigation of universal self-similarity of turbulence quantities in the far wake is a question of interest (Rind and Castro 2012b).

Wake investigations have been performed downstream of different types of disks. Generally, two types of disks can be distinguished: solid disks and porous disks (PDs). Among solid disks are the classical circular disks that have been studied intensively (e.g., Hwang and Baldwin (1966)). Another example of solid disks are fractal disks that have been used to study self-similarity and the decay rate of the mean velocity deficit (e.g., Dairay et al. (2015) and Obligado et al. (2016)). For porous disks, two major types have been used for wake investigations: mesh disks and disks with varying degrees of blockage that can also change radially. Porous disks are interesting to study for their practical use to replicate the flow past, for example, parachutes (Higuchi et al. 1998) or more often wind turbines (España et al. 2011, 2012; Aubrun et al. 2013; Theunissen et al. 2015; Lignarolo et al. 2016; Howland et al. 2016; Camp and Cal 2016; Bossuyt et al. 2017; Yu et al. 2017, 2019; Camp and Cal 2019; Abdulrahim et al. 2021; Helvig et al. 2021; Neunaber et al. 2021; Vinnes et al. 2022). To replicate the flow past a wind turbine, PDs are often mounted to towers which breaks the axisymmetry of the wake by shifting it in the direction of the tower (Pierella and Sætran 2017).

Classically, wake studies were carried out in laminar inflow to investigate the entrainment of flow into the wake without external disturbance. However, in the past years, the interest of the impact of turbulence in the inflow on the evolution of the wake has increased due to, among others, a number of applied problems particularly in the field of wind energy, where the flow a wind turbine experiences is typically turbulent. For turbulent inflow, it can be distinguished between homogeneous inflow turbulence and sheared inflow turbulence like, for example, boundary layer turbulence.

Rind and Castro (2012b) investigated the axisymmetric far wake of a solid disk in homogeneous turbulent flows with different turbulence intensities (TIs). They measured velocities for downstream positions $65 \leq x/D \leq 115$, where D denotes the diameter of the disk and x the distance from the disk. For the control case with a laminar incoming flow, they confirmed the self-similar behavior described by Tennekes and Lumley (1972). However, they showed that an increased incoming TI and length scale in the flow increases the wake momentum deficit and the far wake's velocity decay rate, in addition to delaying or preventing the appearance of self-similarity. Rind and Castro (2012a) also performed a direct numerical simulation (DNS) of a time developing axisymmetric wake. The DNS largely corroborated their experimental findings (Rind and Castro 2012b).

Cannon et al. (1993) performed flow visualizations with porous disks and solid disks in laminar inflow. They used mesh disks with different solidity, and found that vortex shedding could not be observed for disks with solidity below 60%. Higuchi et al. (1998) performed particle image velocimetry (PIV) experiments in laminar inflow in the near wake of PDs with annular slots intended to simulate ribbon parachutes. They found that the flow through the slots created jets that would, depending on the spacing between slots, merge and form high-momentum regions that displaced the reverse-flow region typically found behind solid disks. This resulted in the near-field of the wake being more axisymmetric instantaneously than at the same position for a solid disk. Similar results were obtained by Theunissen and Worboys (2019) for disks with 4-6 annular holes with varying hole diameter in laminar inflow. It has further been shown that an increase in the solidity of a PD increases the rate of the velocity deficit decay and decreases the rate of the wake width expansion (Cannon et al. 1993; Higuchi et al. 1998; Myers and Bahaj 2010; Blackmore et al. 2014; Theunissen and Worboys 2019).

While the aforementioned studies where performed in low freestream TI, a few studies have included the effect of freestream turbulence. Blackmore et al. (2014) placed disks perforated with circular holes in varying incoming turbulent flows. They varied the freestream TI and the integral length scale L, and found that the disks experienced a significant increase in drag with higher turbulence intensity up to a turbulence intensity of around 13%. For higher TI the results became approximately independent of the TI. Aubrun et al. (2013) and Abdulrahim et al. (2021) studied the impact of an atmospheric boundary layer on the evolution of the wake of a disk. Later, Neunaber et al. (2021) experimentally studied the evolution of the turbulence in the wake center of a PD and a wind turbine exposed to different turbulent inflow conditions, also investigating higher-order two-point statistics.

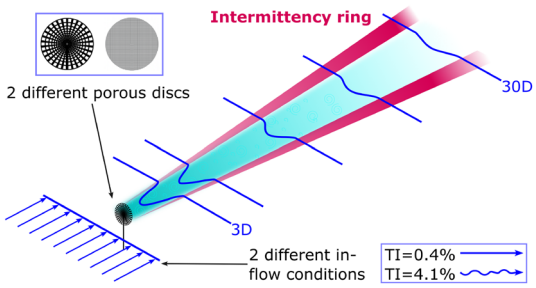

Fig. 1 Experimental overview: the wakes of two porous disks are exposed to two turbulent inflows

The studies above focused on the impact of the turbulence and the disk shape on the evolution of the mean velocity deficit, sometimes also looking at the turbulence or the mixing and energy entrainment to the wake. However, to fully understand the nature of a turbulent flow, it is necessary to include not only mean quantities but also include a measure of the order in which events occur. For example, energy spectra can be used to investigate the type of turbulence or structures in the wake, as the vortex shedding. Also, two-point statistical quantities can be used to identify intermittency, i.e., the "gustiness," of a flow. Schottler et al. (2018) and Neunaber et al. (2020) demonstrated that there is a ring of highly intermittent flow at scales corresponding to the rotor diameter at the outermost part of a wind turbine wake. No such study exists for PDs.

The aforementioned studies investigate either the difference of wakes generated by different porous disks (e.g., Aubrun et al. (2019)) or the impact different degrees of turbulence have on the wake. Typically, the differences are looked at in terms of mean velocity or energy transport. However, a study that combines the investigation of different types of disks with similar solidity and drag exposed to different inflow turbulence intensities with an analysis by means of higher-order two-point statistics is still missing. From this, two research questions arise for this study, namely

1. How do the disk design and the inflow turbulence influence the wake evolution?
2. How does the intermittency evolve in the wake of a porous disk with respect to different time scales?

We will address these research questions with the following research objectives (also illustrated in Fig. 1):

- Use two PDs (one of each design type, i.e., mesh design and radially varying design)
- Generate two different turbulent inflows
- Perform measurements between $3 \leq x/D \leq 30$ to cover the transition from near wake to far wake
- Investigate the results by evaluation of the mean velocity and turbulence intensity, time series, energy spectra, and intermittency

In this paper, we will give an overview of one-point and two-point statistical quantities in Sect. 2. The experimental setup is presented in Sect. 3 and the results are discussed in Sect. 4. Finally, the main findings are summarized in the conclusion in Sect. 5.

2 Theory

In the following, the analysis methods used to characterize the measured flow fields are introduced. To properly motivate the characterization of the intermittency by means of the shape parameter, this section details both the common analysis using one-point statistical quantities and the analysis using two-point statistical quantities. The structure of this section is taken up in the results section. We will summarize the descriptions given in Morales et al. (2011) and Neunaber et al. (2021).

2.1 One-point statistics

Often, the time series of flow velocities $u(t)$ measured at times t is decomposed into the mean flow velocity U and the fluctuations around the mean $u'(t)$[1],

$$u(t) = U + u'(t). \tag{1}$$

The variance $u'^2 = \frac{1}{N}\sum_{t_1}^{t_N} u'^2(t)$ characterizes the strength of the fluctuations, which are also often quantified with respect to the mean velocity as the turbulence intensity, u'/U. As the calculation of the quantities U and u'^2 does not depend on the order the values of $u(t)$ occur in, they are called one-point statistical quantities or, rather, "one-time" statistical quantities.

We would like to point out that the nth moment of a quantity $q(t)$ is denoted as Q^n. If the probability density of this quantity, $p(q(t))$, follows a Gaussian distribution, the complete one-point statistical behavior of $q(t)$ is described by Q and Q^2. Therefore, the mean flow velocity U and the variance u'^2 are the first and second moment of the flow velocity, also referred to as first- and second-order one-point statistical quantities, and their one-point statistical behavior is completely characterized by U and u'^2 if $p(u(t))$ follows a

[1] Note that here, a quantity depending on the time is denoted as $q(t)$ while the time average of this quantity is denoted as Q.

Gaussian distribution. The sequence of the events does not play a role for this description, i.e., the characterization of a signal in random and sorted sequence give the same one-point statistical information (e.g., figure 3 in Morales et al. (2011)).

2.2 Two-point statistics

One-point statistical quantities give a good overview of mean quantities such as the mean velocity or turbulence intensity of a turbulent flow. However, the sequence in which events occur is neglected by this type of characterization, but for the description of turbulence, this information is relevant (e.g., Morales et al. (2011)). Therefore, to also include the impact of the sequence in which events occur, two-point, or two-time, statistical quantities are needed as they characterize a quantity with respect to two times t and $t+\tau$ that are separated by a fixed step τ.

The autocorrelation function

$$R_{uu}(\tau) = \frac{1}{u'^2}\left\langle u'(t+\tau)u'(t)\right\rangle, \tag{2}$$

where $\langle\cdot\rangle$ denotes averaging in time, is one choice to include the order of events. $R_{uu}(\tau)$ is, via the Fourier transform $\mathscr{F}$, directly related to the energy spectral density $E_{uu}(f)$ by means of the Wiener–Khintchine theorem,

$$E_{uu}(f) \overset{\mathscr{F}}{\longrightarrow} R_{uu}(\tau).$$

Therefore, $E_{uu}(f)$ is a second-order two-point statistical quantity and it indicates the energy present at a certain frequency of the signal. Further, $u'^2 = \int E_{uu}(f)\mathrm{d}f$ denotes the energy in the signal.

A lot of information about a flow can be drawn from the data using $E_{uu}(f)$ in combination with U and u'^2. However, some features such as the turbulence intermittency can only be identified using higher-order two-point statistics. Note that, while the term intermittency is also used for a flow that varies between turbulent and laminar states, here, we use it to describe the occurrence of extreme events, or gusts, in a fully developed turbulent flow. In Pope (2000), this type of intermittency is referred to as *internal* intermittency, and when discussing intermittency in this work, we always refer to internal intermittency. Therefore, it is not sufficient to investigate the flatness of the velocity to characterize intermittency. For this, we introduce the central velocity increment $\delta u_\tau(t) = u(t-\tau/2) - u(t+\tau/2)$ that represents the difference of two velocities at times $t-\tau/2$ and $t+\tau/2$ with respect to a time scale τ. The investigation of intermittency is often done by looking at the structure functions, defined as the moments of the velocity increments δu_τ^n (e.g., Kolmogorov (1962); Toschi et al. (1999); Pope (2000)). Similar to Morales et al. (2011) and Neunaber et al. (2021), we will, however, focus here on a different way of investigating intermittency: the probability density function of velocity increments $p(\delta u_\tau(t))$ that also includes the complete information of δu_τ^n. If $p(\delta u_\tau(t))$ follows a Gaussian distribution, then only the first two moments (δu_τ^n with $n = 1, 2$) are needed to describe the complete two-point statistics of the flow. However, it has been shown that in some turbulent flows, the probability of large velocity fluctuations (i.e., extreme events) is significantly higher than predicted by a Gaussian distribution. This is typical of turbulence intermittency. To quantify the deviation of $p(\delta u_\tau(t))$ from a Gaussian distribution, we use the shape parameter

$$\lambda^2(\tau) = \frac{\ln\left(F\left(\delta u_\tau(t)\right)/3\right)}{4} \tag{3}$$

as introduced by Chillà et al. (1996) where

$$F(\delta u_\tau(t)) = \frac{\langle(\delta u_\tau(t))^4\rangle}{\langle(\delta u_\tau(t))^2\rangle^2} \tag{4}$$

is the flatness of $\delta u_\tau(t)$. As discussed in further detail in Appendix A, the advantage of this approach is that an explicit expression for the statistics of $p(\delta u_\tau(t))$ exists (Castaing et al. 1990).

Analyzing the velocity fluctuations by means of the energy spectral density that supplies the variance of $p(\delta u_\tau(t))$ in combination with the shape parameter λ^2 of $p(\delta u_\tau(t))$ provides a complete statistical two-point characterization. If $\lambda^2 \approx 0$, $p(\delta u_\tau(t))$ follows a Gaussian distribution and the flow is non-intermittent. If $\lambda^2 > 0$, $p(\delta u_\tau(t))$ deviates from a Gaussian distribution and the flow is intermittent at the respective time scale τ.

3 Experimental procedure

The experiments were performed in the large closed-loop wind tunnel at the Norwegian University of Science and Technology (NTNU), where the test section has dimensions of 11.15 m × 2.71 m × 1.80 m (length × width × height). The roof was adjusted so that the height gradually increases to 1.85 m at the outlet. This compensates for the growing boundary layers and ensures that the pressure gradient in the streamwise direction is approximately zero. A schematic of the experimental setup can be seen in Fig. 2.

Two different inflow turbulence levels were generated for this study, a high TI case and a low TI case. For the high TI cases, a bi-planar wooden grid was installed at the entrance of the test section (marked as grid position 1 in Fig. 2). The wooden grid has a mesh length $M_1 = 242$ mm and a solidity of 35%, and is the same as the uniform grid used by Bartl and Saetran (2017) and Bartl et al. (2018). A wire mesh screen was used to homogenize the flow, mounted

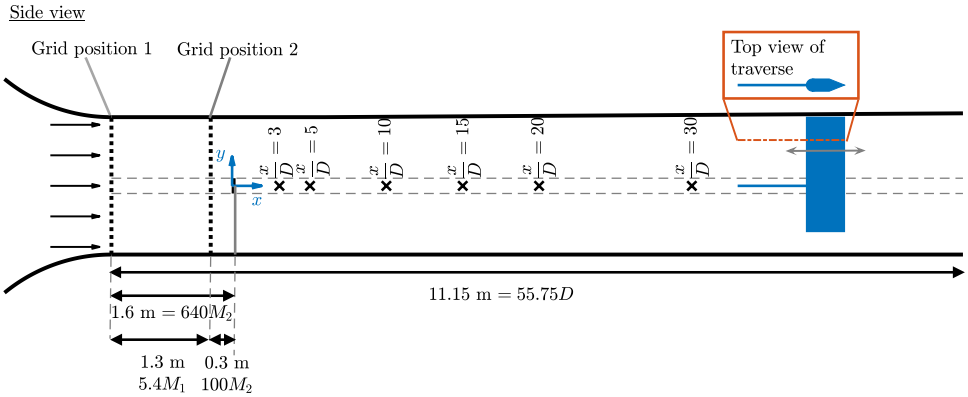

Fig. 2 Schematics of the experimental set-up. The streamwise measurement positions are marked by ×. For the low TI measurements, the wire mesh was located at the start of the test-section at grid position 1. For the high TI measurements it was moved to grid position 2, while a wooden bi-planar grid was positioned at grid position 1

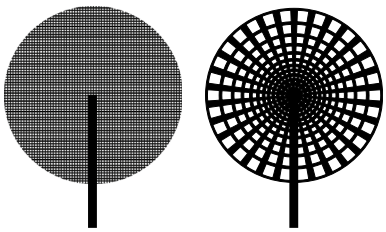

Fig. 3 Illustration of the UD (left) and ND (right)

1.3 m downstream of the bi-planar grid at grid position 2. The wire mesh has a mesh length of $M_2 = 2.49$ mm and a solidity of 34%. The TI and integral length scale with this setup were measured to be 4.1% and 0.3–0.4 m, respectively, at the position of the disks. As this is a turbulent flow, we find small intermittency values for small scales of τ but for scales corresponding to 80 mm ($0.4D$) or larger, the flow is non-intermittent

For the low TI measurements, the wooden grid was taken out and the wire mesh was moved to grid position 1, resulting in an average TI over the wind tunnel span of 0.4% at the disk location. As this is a very low turbulent flow, no intermittency is present.

The two PDs both have a diameter of $D = 200$ mm, yielding a Reynolds number of $Re = \frac{U_\infty D}{\nu} \approx 1.1 \times 10^5$ for the experiments, where $U_\infty = 8.1\,\mathrm{ms}^{-1}$ is the freestream velocity and ν is the kinematic viscosity. The disks are the same as the ones used by Vinnes et al. (2022). The schematics of them are shown in Fig. 3. The uniform disk (UD) was also used by Aubrun et al. (2019), while the non-uniform disk (ND) is inspired by the disk of Camp and Cal (2016, 2019) that was also the second disk of Aubrun et al. (2019). Both disks have a solidity of 57% and a drag coefficient $C_D \approx 0.8$. The UD is made out of a wire mesh with uniform blockage, while the ND is cut from a 5 mm acrylic sheet, and the blockage is reduced with increasing distance from the center. The disks were mounted on a tower and positioned in the center of the tunnel. More details on the disks and mounting can be found in Vinnes et al. (2022).

The data acquisition and post-processing were done in the same manner as by Vinnes et al. (2022), and the methodology is described in detail there. Therefore, only a summary will be presented here. The data was collected through 1d hot-wire anemometry (HWA) at six downstream positions (see Fig. 2). For each downstream position, a full wake scan was performed. Half the wake was scanned with a measurement spacing of 10 mm and a sampling time of 360 s. The other half was measured with a sampling time of 200 s to check for symmetry. The spacing between measurement points was larger on this side, which will be visible in the wake profiles. The sampling frequency was set to 30 kHz. This was sufficient to capture the full velocity spectra down to the advection frequency of the Kolmogorov length scale, which was estimated to have a maximum of $f_\eta = 8.5$ kHz. An analog low-pass filter was applied at 10 kHz, and the iterative digital low-pass filtering methodology of Mi et al. (2005, 2011) was used for each individual measurement to reduce remaining high frequency noise. The length of the wires (1.25 mm) is on the order of the longest Kolmogorov length scale of $\eta_{\max} = 1.1$ mm.

Two or three wires were used for simultaneous acquisition and the temperature was measured simultaneously. The voltage signal was converted to velocity through using a fourth-order polynomial, and the temperature correction methodology of Hultmark and Smits (2010) was used; this technique was demonstrated to compensate for temperature variations up to 15K. The calibration coefficients were calculated at the beginning and end of each day of the campaign, and a weighted average was used for the measurements taken in between; the calibration curves typically collapsed after applying temperature correction and data that did not meet this criteria were discarded and re-measured. For each wake scan, the measurements outside the wake region on each side were used to correct for both individual wire drift and inter-wire drift.

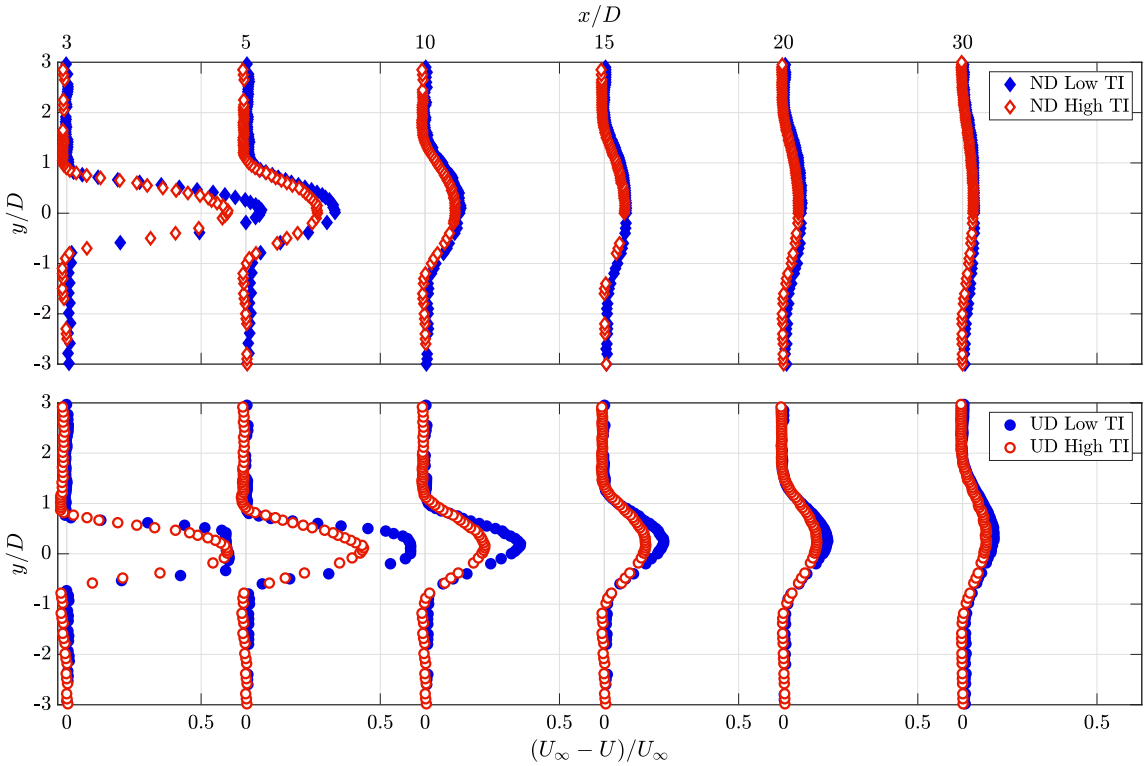

Fig. 4 Normalized velocity deficit in the ND wake (top) and UD wake (bottom) for the different incoming turbulence intensities

4 Results and discussion

Vinnes et al. (2022) performed an analysis on the wakes of the PDs in low turbulent flow. This paper expands that work by investigating the wakes in turbulent incoming flow. Furthermore, two-point statistical quantities are described in greater detail. In the following, the velocity deficit and TI will be presented as one-point statistical quantities in the wakes, followed by a discussion of the two-point statistics with focus on λ^2.

4.1 One-point statistics

The normalized mean velocity deficit in the wakes of both disks is shown in Fig. 4, for both high and low incoming turbulence. The wakes drift slightly to positive y-values as they propagate downstream. The shift is less than 2% of the distance from the disks. This is due to a small velocity gradient in the background flow, less than 1% across the wind tunnel. For the purpose of this paper, this drift was deemed acceptable, and no corrections for it have been made. Fig. 4 is designed to give an overview of the evolution of the wake. To get a better impression of the quantitative values, the profiles are plotted on a larger scale in Appendix B.

For the ND, the increased turbulence intensity reduces the velocity deficit. Close to the disk, for $x/D \leq 5$, the largest difference between the low and high turbulent cases is in the center of the wake, while farther downstream, the difference in the velocity deficit is largest around the edges, i.e., the wake width is smaller for the high turbulent case. The shape of the wake is similar to a Gaussian curve for all positions for both the high and low TI case, and is not altered much by the freestream turbulence.

In contrast to the ND wake, the incoming turbulence changes not only the wake recovery, but also the shape of the UD wake. At $x/D = 3$, where the low TI case displays a top hat profile, the incoming turbulence enhances the development of the shear layers, such that they almost meet. $5D$ downstream of the UD in high TI, the shear layers meet, forming a profile with a pointed shape, before it turns Gaussian-shaped farther downstream. For the low TI case, the pointed profile appears at $x/D = 10$, showing how the UD wake develops faster in high freestream turbulence. At all positions, except $x/D = 3$, the maximum velocity deficit is substantially reduced by the high freestream turbulence. The maximum reduction in velocity deficit is more pronounced as compared to the ND case. It is as such evident that the UD wake is more significantly influenced by the freestream turbulence levels.

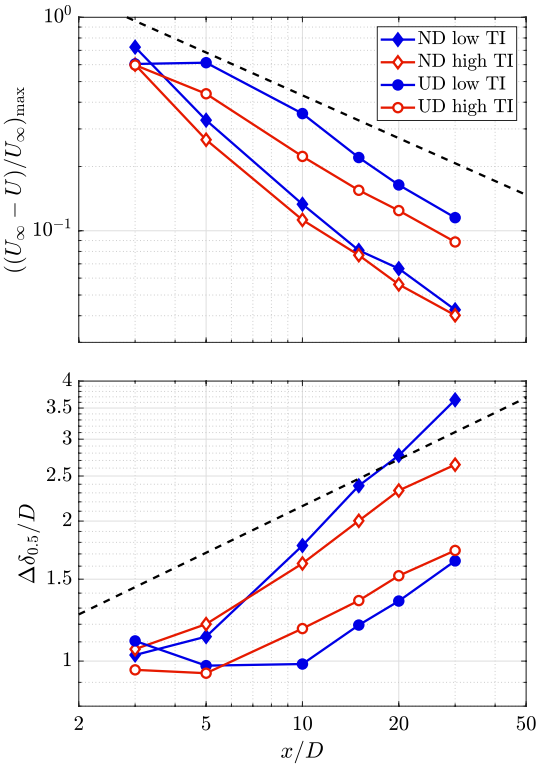

Fig. 5 Evolution of the maximum velocity deficit (top) and the wake half-width (bottom) with increasing downstream distance. The dashed lines represent the theoretical evolution of an axisymetric wake, $x^{-2/3}$ for the velocity deficit and $x^{1/3}$ for the half-width (George 1989)

Figure 5 shows a more quantitative approach to evaluating the wakes, displaying the streamwise evolution of the maximum velocity deficit (top panel) and the wake half-width (bottom panel). As observed in Fig. 4, the freestream turbulence reduces the maximum velocity deficit for the wakes. Generally, the reduction is higher for the UD. The only exception is for the UD at $x/D = 3$, but the UD wake in low TI inflow is still developing at this point; there is still significant turbulence production in the shear layers. From $x/D = 3$ and $x/D = 5$, for the ND and the UD, respectively, and farther downstream, the evolution of the maximum velocity deficit approximately follows a power law. A qualitative comparison with the analytical prediction of the decay of the mean velocity deficit for a turbulent axisymmetric far wake of a bluff body, $x^{-2/3}$ (George 1989), indicated by the dashed line in Fig. 5, reveals the present flows do not necessarily agree with these predictions. This occurs for numerous reasons, including that the measurements include the transition from near to far wake, the bodies are porous rather than the canonical bluff body, and that the downward shift in the wake caused by the tower (Pierella and Sætran 2017; Aubrun et al. 2019), moving the wake centreline away from the geometric centreline. Therefore, we forego a quantitative comparison with analytical expectations (Pope 2000) that are essentially for a different flow.

The wake half-width, $\Delta\delta_{0.5}$, is here defined in the same manner as Rind and Castro (2012a, 2012b), i.e., the distance between the two locations where the velocity deficit is half the maximum velocity deficit. As expected for an axisymmetric turbulent far wake, the expansion follows a power law from $x/D = 10$ for the ND and high TI UD cases and $x/D = 15$ for the low TI UD case. For all cases, from $x/D = 10$ the wake width grows slower for the high TI inflow than for the low TI inflow. The turbulent–turbulent interface work of Kankanwadi and Buxton (2020) suggests this is related to a reduction in entrainment caused by the presence of turbulence in the surrounding flow. A qualitative comparison with the analytical prediction of the decay of the wake width for the turbulent axisymmetric far wake of a bluff body, $x^{1/3}$ (George 1989), indicated by the dashed line in Fig. 5, reveals deviations from canonical expectations. However, these are related to the aforementioned differences between the present flow and the canonical one used in the analytical derivations.

The TI profiles of the different wakes are shown in Fig. 6. As for the velocity deficit, the profiles are shown on a larger scale in Appendix B. The TI decay in the freestream downstream of the grid is visible, and at $x/D = 30$ the high TI flow barely displays higher turbulence than the low TI flow. For the ND at the nearest measurement positions, $x/D = 3$ and $x/D = 5$, the maximum TI in the wake is lower for the high TI inflow, but the levels equalize farther downstream. At the first measurement position, the profiles are Gaussian-like, while they have a profile with a plateau in the center for the farther downstream positions. The UD wake develops more slowly to this plateau shape, and for the low TI inflow, it does not reach such a state before $x/D = 15$. Closer to the disk the profiles display two peaks in the shear layers. The shear layers have not yet met, and there is thus no turbulence production in the center of the wake. The turbulence levels in the UD wake remain higher for the low TI case from $x/D = 10$ throughout the measurement domain because of the slower wake evolution where turbulence takes longer to build up.

The described observations show that the ND wake, both in low and high freestream TI, has reached a developed state at $x/D = 10$, and perhaps already at $x/D = 5$. This indicates that the turbulence evolution is enhanced in the wake of the ND as compared to the UD wake, likely due to high turbulence production fueled by jets in the near wake as a result of the disk design. From this point, both the maximum velocity deficit and the wake half-width follow a power law, and the shape of the velocity deficit and TI profiles are not changed significantly. As indicated above, the turbulence changes the exponents

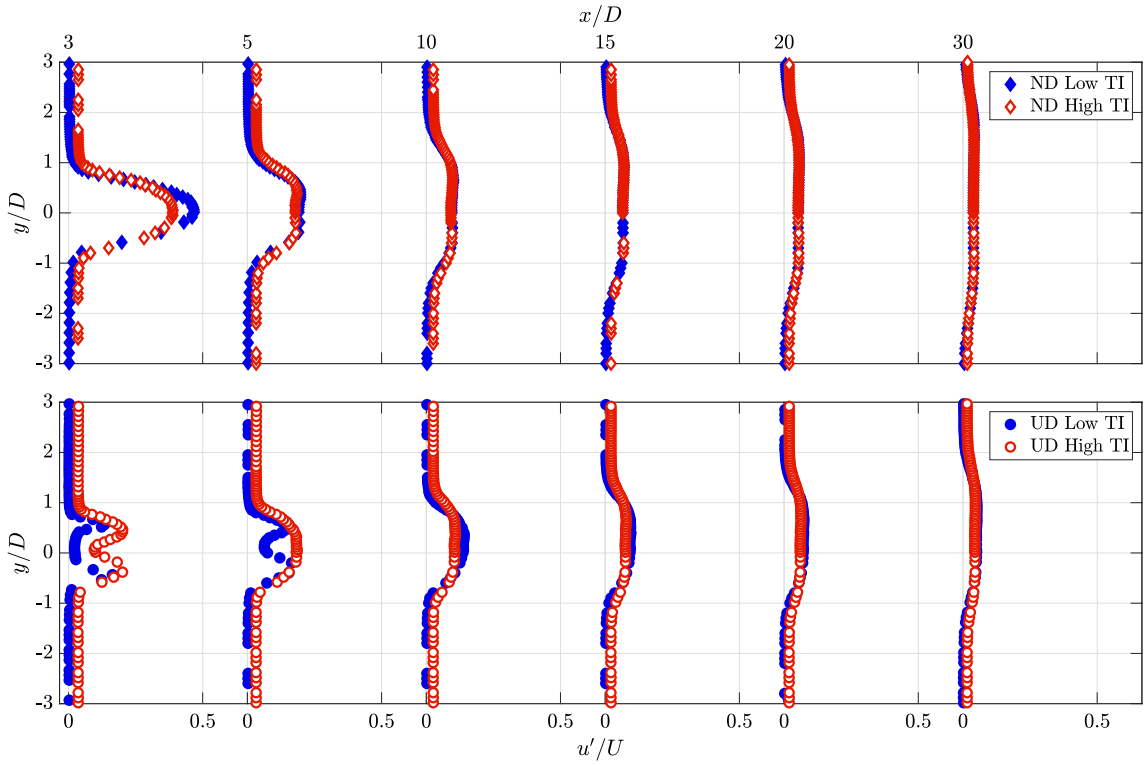

Fig. 6 Turbulence intensity in the ND wake (top) and UD wake (bottom) for the different incoming turbulence intensities

of the power laws, i.e., it reduces the wake expansion and velocity recovery rate. However, this might, at least partly, be due to the effect of the tower. Furthermore, the freestream turbulence changes the velocity and TI magnitudes, i.e., they are reduced.

The UD wake in low freestream TI reaches a developed state at $x/D = 15$. From this position, both the recovery rate of the centerline velocity and expansion rate of the wake are more rapid than for the high TI case. The development of the wake from two thin shear layers to the point where they meet is enhanced by the higher freestream turbulence. This effect might also exist for the ND, but closer to the disk and upstream of the measurements in the present work. The change in the magnitudes of the velocity deficit and TI are also more prominent for the UD wake compared to the ND case. A reason for this may be that, similar to screens used in a wind tunnel to homogenize the flow, the UD acts as a "flow homogenizer" due to the fine grid. As a consequence, turbulent mixing is not fueled from turbulence within the wake but only driven by turbulence from the inflow (in high TI inflow) and the shear layers. Low turbulent flow in the center of the UD's near wake illustrates the low turbulence production in this region where the shear layers, indicated by peaks of high TI, have not yet met. Once the shear layers have met, around $x/D = 10$ downstream, the turbulence production is fueled which is indicated by the increasing TI levels at $x/D = 15$, and then the turbulence decays. The inflow turbulence does accelerate and dampen this behavior (indicated by the lower TI levels in the wake from $x/D = 10$). The ND generates turbulence due to the strong jets in the near wake that are more persistent and enhance turbulent mixing, which accelerates the wake evolution, and the additional impact of the ambient turbulence is reduced.

4.2 Two-point statistics

To have a better understanding of the turbulence evolution in the wakes, we will complement the discussion of the mean velocity deficit and turbulence intensity by looking into structures present in the flow using two-point statistical quantities. To visualize the importance of an analysis that includes also the order of events, snippets of the velocity time series are shown in Fig. 7 for the ND and Fig. 8 for the UD. The time series are taken at three different spanwise positions at $x/D = 10$. We chose this downstream position for two main reasons: first, this distance is of interest for the wind energy community as it approximately represents typical spacing within a wind farm; second, the turbulence of the wakes is well developed but does not expand too far allowing for investigation both inside and outside the wake. The top panel of each of the figures display the velocity at

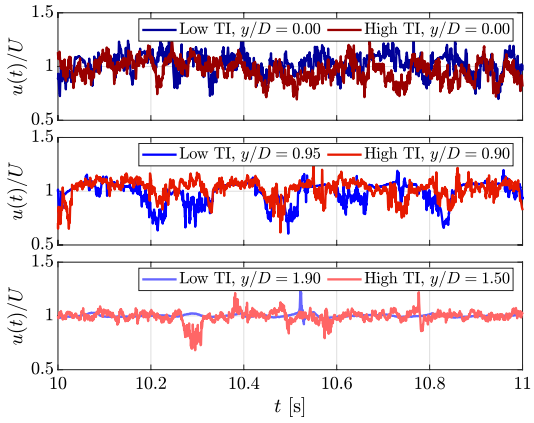

Fig. 7 Time series at $x/D = 10$ for the ND. The panels show the centerline (top), shear layer (center), and outermost (bottom) spanwise positions

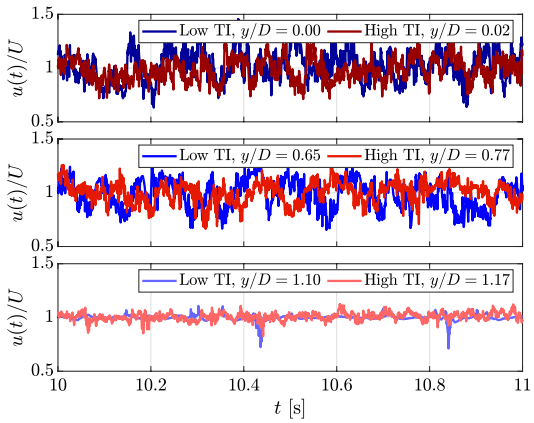

Fig. 8 Time series at $x/D = 10$ for the UD. The panels show the centerline (top), shear layer (center), and outermost (bottom) spanwise positions

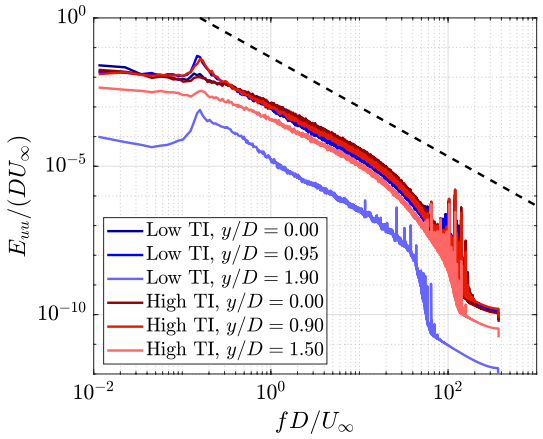

Fig. 9 Streamwise velocity spectra for chosen spanwise positions at $x/D = 10$ for the ND. The dashed line indicates the Kolmogorov −5/3 law

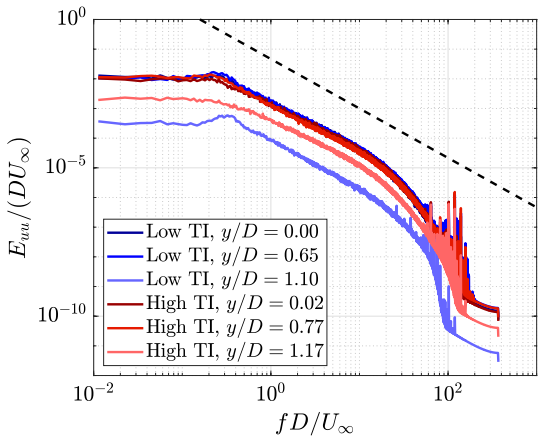

Fig. 10 Streamwise velocity spectra for chosen spanwise positions at $x/D = 10$ for the UD. The dashed line indicates the Kolmogorov −5/3 law

the centerline of the wakes, while the center panels show time series at the position where the velocity deficit is half the maximum velocity deficit. Schottler et al. (2018) showed that there is a region of highly intermittent flow surrounding the low velocity region of the wake, that is, there is intermittent flow outside of what would be defined as the wake based on the velocity deficit alone. Therefore, the bottom panels display the velocity time series at a position just outside the wake where the velocity deficit is approximately zero. Due to the different width of the wakes, the two latter positions differ between the disks and ambient TIs, but the physical positions are shown in the legends. For example, the shear layer position plotted in the center panel of Fig. 7 is $y/D = 0.95$ for the low TI case and $y/D = 0.90$ for the high TI case as the position where the velocity deficit is half the maximum velocity deficit is different for the two cases.

At the centerline (top panel) for the ND (Fig. 7), there are no visible periodic structures. However, the turbulent fluctuations of the flow are evident. The same is observed for the UD in Fig. 8, where the flow is clearly turbulent, but still without any visible periodicity. The low TI case has larger fluctuations, and thus higher TI, which agrees with the TI profiles in Fig. 6.

There are more prominent differences between the disks in the time series obtained in the shear layer. For the UD, the flow is still turbulent, with no distinguishable pattern in the fluctuations. In contrast, the flow in the ND wake seems to alternate between two states; one turbulent state with reduced mean velocities and strong fluctuations and one less turbulent state with higher time-averaged velocities but smaller fluctuations. In the low TI case, the flow appears to be close to laminar between the turbulent, low velocity

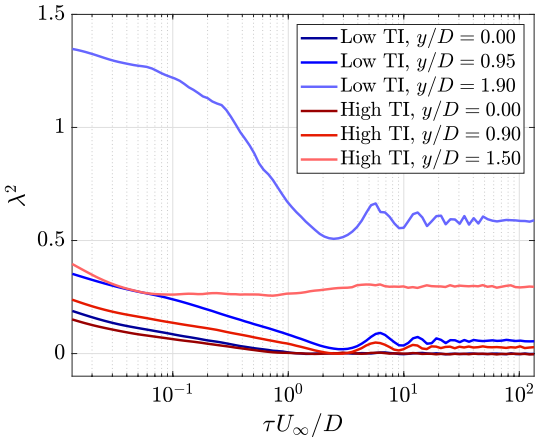

Fig. 11 Shape parameter λ^2 for chosen spanwise positions at $x/D = 10$ for the ND

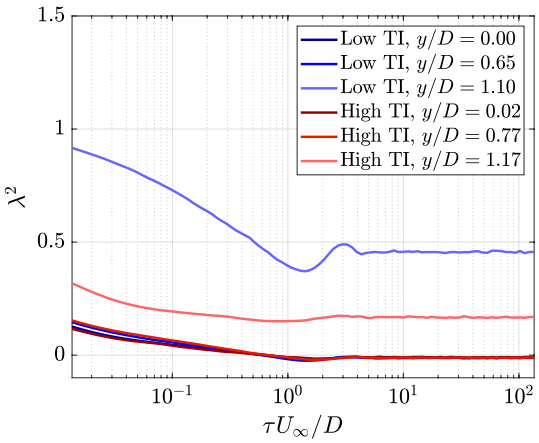

Fig. 12 Shape parameter λ^2 for chosen spanwise positions at $x/D = 10$ for the UD

events. The freestream turbulence reduces the distinction between the two states. It is, however, still present.

At the outermost position, the flow is mostly uniform, either close to laminar for the low TI cases or with some turbulence for the high TI case. The velocity is either reduced or increased in some short bursts, clearly indicating that the flow is intermittent, suggesting that the ring of highly intermittent flow around the wind turbine wake (Schottler et al. 2018) is also present for PD wakes. The time snippet used in Figs. 7 and 8 is not sufficiently long to say anything about how often these bursts occur or if there is any periodicity.

To analyze the periodicity of events in the flow, it is useful to investigate the energy spectral density, or, simply, the velocity spectra, at different transverse positions in the wake. They are shown in Figs. 9 (ND) and 10 (UD) with respect to the reduced frequency fD/U. In case of the ND, a distinct peak with a reduced frequency of $fD/U = 0.15$ (low TI) and $fD/U = 0.16$ (high TI) is visible particularly at outer radial positions. Vinnes et al. (2022) showed that the frequency in the low TI case is the shedding frequency of the ND. With only a minor change of frequency, the peak for the high TI case is ascribed to the same phenomenon. The strength of the shedding is independent of the inflow TI in the shear layer. In contrast, the shedding peak is barely visible in the high TI case at the outermost position, whereas it is clearly visible in the low TI case.

In the spectra in the wake of the UD in Fig. 10, no vortex shedding peak is visible. This was also shown by Vinnes et al. (2022). Although there is no distinct peak, a broadband range of more pronounced frequencies appear around $fD/U = 0.2 - 0.4$ as a "bump," identified by Vinnes et al. (2022) as structures arising from the strong shear gradients. The energy content of this bump is reduced slightly for the high TI case. This is consistent with the velocity deficit profiles in Fig. 4, which show that the shear gradient is reduced with higher ambient turbulence, and thus the structures stemming from the shear have less energy.

For both disks, it can be observed that more energy is present for all frequencies in the wake than outside of the wake. In the center, the spectra in high and low TI inflow collapse which means that the turbulence at the wake centerline is independent of the inflow turbulence, which has also been shown by Neunaber et al. (2021). A direct comparison of the spectra at the centerline for all disks and inflow conditions reveals that, as the spectra are similar for small frequencies and collapse for the inertial sub-range, the turbulence also becomes independent of the disk, which is in accordance with the findings of Neunaber et al. (2021) for the wakes of a PD and a wind turbine.

To include the intermittency in the flow, Figs. 11 and 12 show the shape parameter λ^2 over a range of scales τ for the ND and the UD, respectively. For consistency, the same spanwise positions used in Figs. 7, 8, 9 and 10 are investigated.

For all measurement cases, the centerline behavior agrees with the measurements by Neunaber et al. (2021), showing some intermittency at small time scales, before converging to zero for larger time lags. Considering that their measurements were taken closer to the disk, the agreement with Neunaber et al. (2021) is good. At the outermost positions, the values are higher for small τ and converge to $\lambda^2 > 0$ for large time lags τ. Note that the high values of λ^2 for very small τ in the shear layers originate from an application of the phenomenology to a flow that is not fully turbulent and has small standard deviations $\langle(\delta u_\tau)^2\rangle$. While the calculation of λ^2 will still give an indication of the existence of intermittency (both internal intermittency and "classical" intermittency), the Castaing distributions may not approximate the probability density function of δu_τ satisfactorily (see Appendix A). For the current profiles, this only happens

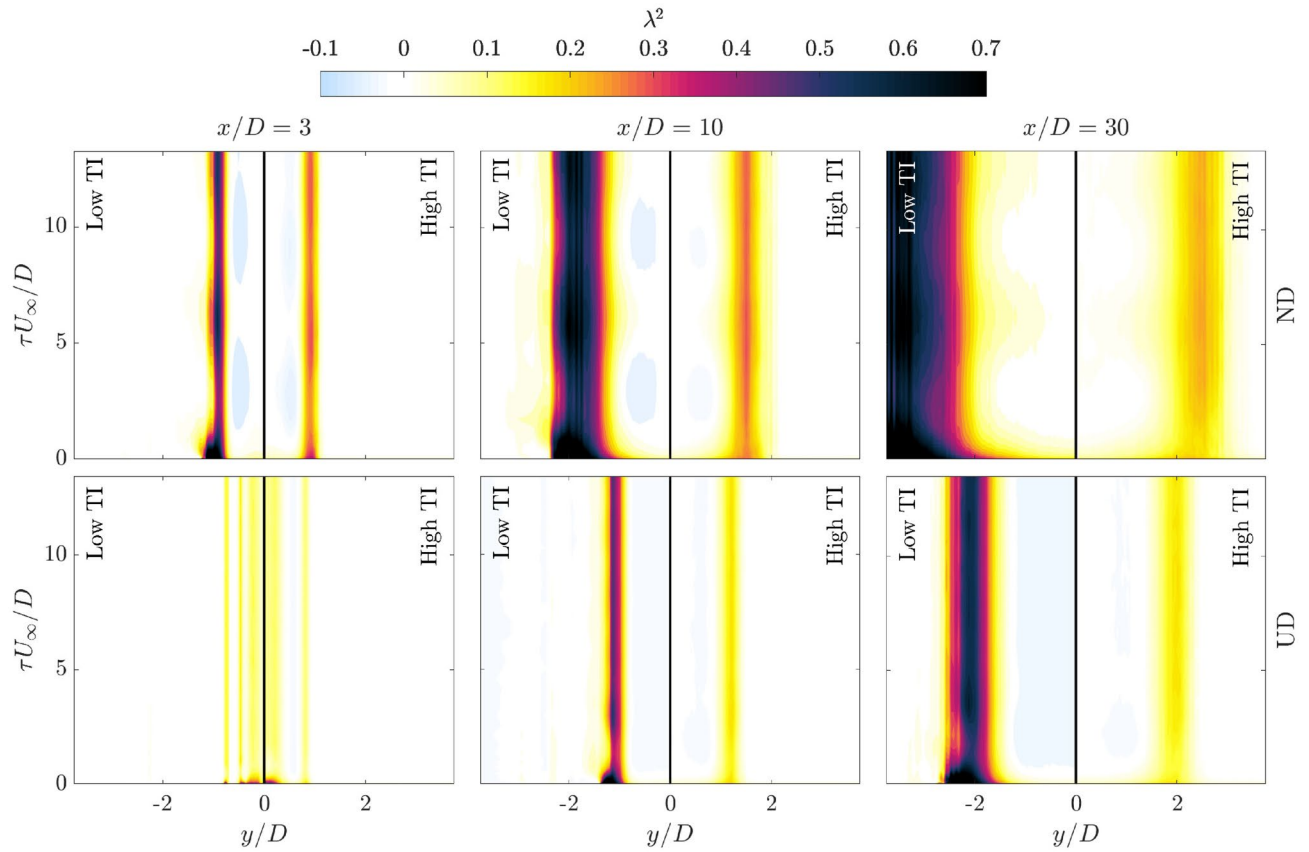

Fig. 13 The shape parameter λ^2 plotted for all y-positions over time lags τ for $x/D = 3$, 10, and 30, from left to right, respectively. Top row: ND, bottom row: UD. In each figure, the low TI measurements are mirrored and plotted on the negative y-axis, although the presented results are from the side with high density measurement positions

for the very small τ. In the shear layer, λ^2 follows the centerline values for the UD. In contrast, in the ND wake, the values are higher in the shear layer than at the centerline. At all measurement positions, for all cases, the values converge for high τ. This is not surprising. In fact, when the time lag is longer than the longest correlation scales in the flow, λ^2 should become independent of τ.

The most striking observation in Fig. 11 is perhaps the periodic lines in the shear layers and for the outermost position in the low TI case for the ND, which are not present for the UD in Fig. 12. The explanations for the periodic lines can be found in the velocity spectra in Fig. 9. The positions that have periodic lines also have a peak in the velocity spectra. If this reduced frequency is translated into time scale, the first peak in the λ^2 profiles has approximately the corresponding time lag, namely $\tau U_\infty/D = 6.3$ (low TI) and $\tau U_\infty/D = 5.7$ (high TI). Thus, the flow at these positions is more intermittent at the shedding frequency and the harmonics of it compared to frequencies in between. With a time lag corresponding to the vortex shedding, the velocities $u(t + \tau/2)$ and $u(t - \tau/2)$ used to calculate the velocity increment δu_τ will be taken at roughly the same position in two following vortices. As such, the velocity increment will typically be small. Due to small deviations in the time (or distance) between two vortices, some of the increments at this time lag will be larger, reaching extreme values. This leads to a distribution of δu_τ that has a low standard deviation, but with extreme events, yielding high flatness and λ^2; this is because of the definition of the flatness where the standard deviation is used for normalization. The same is true for the harmonics, but with more than one vortex in between the $u(t \pm \tau/2)$. In contrast, the local minima represent a time lag of half a vortex (or one and a half and so on). Then $u(t + \tau/2)$ and $u(t - \tau/2)$ will always be taken in opposite positions, yielding high values of δu_τ of both positive and negative sign. Thus, the standard deviation is high and the flatness and λ^2 becomes low. In the flow, this means that the extremes seen at the τ with higher λ^2 are not necessarily larger than the fluctuations at τ with lower λ^2, but the large standard deviation still makes it less intermittent. λ^2 can therefore be an indicator of periodic structures present in the wake.

At the outermost positions for both disks, the high TI case reduces the intermittency significantly, in particular for

small τ, but λ^2 also converges to values larger than zero. This is a direct consequence of the way λ^2 is calculated (Eq. 3). The flatness of δu_τ is, by definition, normalized by the standard deviation of the velocity increment, $\delta u'_\tau$. At the outermost position the time series (see Figs. 7 and 8) show that the measurements are mostly taken in the freestream, with occasional extreme events reaching the measurement position. As such, the standard deviation of the velocity at this position is low as can be seen in Fig. 6. The same holds for the standard deviation of the increment time series $\delta u'_\tau$. In turn, λ^2 reaches high values. The added TI in the freestream increases $\delta u'_\tau$, and, thus, reduces λ^2. This is the definition of an intermittent flow, with rare extreme events having much larger magnitude than most of the fluctuations. As a note, this effect is also to some extent present for the shear layer position in the ND wake. The time series (cf. Fig. 7) reveal high turbulence events in between the low velocity, thus, the flow has a comparable TI to the freestream, which, in the manner described, affects λ^2.

Expanding the analysis to the entire wake at different positions, Fig. 13 shows the shape parameter λ^2 at $x/D = 3, 10,$ and 30, for all y-positions and a range of τ. In the center of the wake, $\lambda^2 \approx 0$ except for very small scales τ. A small region of high values of λ^2 is visible in all of the plots. This marks the edge of the wake, as we have seen before. This is in agreement with the ring of highly intermittent flow around the edge of a wind turbine wake, as described by Schottler et al. (2018), but their result are expanded here to a large range of scales τ. The current results show that the region of highly intermittent flow is more pronounced for the low TI case, both in magnitude, as was discussed earlier, and for the spatial extent in spanwise direction. Furthermore, the width of the intermittent region grows with downstream distance. It is also wider for the ND wake compared to the UD wake. Only for the UD at $x/D = 3$, the described behavior differs. Here, intermittent flow is also present in the center of the wake. However, the TI levels are low at this position due to low turbulence production as the shear layers have not yet met. As discussed earlier, the low TI levels enhance intermittency, as single extreme events are more prominent compared to the background turbulence.

5 Conclusions

A study of the impact of freestream turbulence on the wakes of a uniform and a non-uniform porous disk has been presented. In particular, the evolution of the wakes has been described through one-point turbulence statistics, and structures in and intermittency of the wakes have been investigated by two-point statistics.

At six downstream positions spanning a decade of the evolution between 3D and 30D, the mean velocity and TI profiles have been presented. The results show that higher TI inflow accelerates the wake recovery for both disks when looking at the global evolution of the centerline mean velocity deficit, however, it is increased more for the uniform disk than for the non-uniform disk. This could be due to the enhanced turbulence evolution in the non-uniform disk near wake, where the strong jets cause high turbulence production and, thus, higher turbulence intensity. In contrast to the non-uniform disk, low turbulent flow in the center of the uniform disk's near wake illustrates the low turbulence production in this region where the shear layers, indicated by peaks of high TI, have not yet met. In addition, we observe that the wake width increases more slowly for the high TI inflow in the power-law regime than for the low TI inflow, which we interpret as a reduction of turbulent momentum transport from the ambient flow to the wake due to smaller differences between the TI of the background flow and the TI of the wake.

The vortex shedding observed in some velocity spectra of the non-uniform disk can also be identified in corresponding plots of the shape parameter $\lambda^2(\tau)$. At time lags τ corresponding to the shedding frequency and its harmonics, the intermittency displayed is higher than for τ in between these harmonics, leaving a wavy pattern in the λ^2-plots.

By means of the energy spectra and the shape parameter, we show that sufficiently far downstream, where the shear layers of the wake have met, the centerline turbulence is independent both of the incoming turbulence and the disk design. This confirms theoretical expectations and earlier findings in (Neunaber et al. 2021), who found that the turbulence in the developed regions of wakes downstream of a porous disk and a wind turbine is independent of the wake-generating object and the incoming flow. Furthermore, in the same regions, we show that the intermittency ring found in the outermost parts of the wake of a wind turbine (Schottler et al. 2018) also exists in porous disk wakes, and we confirm its existence for an extended range of scales τ. As such, these features and phenomena are more general than perhaps originally suspected as they were previously documented in detail solely for wind turbine wakes.

At the centerline, intermittency is only present at small scales τ and not for most of the tested range of τ, which is typical for a fully developed turbulent flow. The width and strength of the intermittency ring depend on incoming turbulence and the design of the porous disk, showing that the turbulence's characteristics at the edge of the wake depend on the wake-generating object and the ambient turbulence.

In summary, we find that the wakes of the two different disks are affected differently by the inflow TI, as the wake generated by the UD is more sensitive to it than that of the ND. We have described new features of the turbulence, particularly the intermittency, in the shear layer and the outermost regions of porous disk wakes. For practical applications, i.e., wind turbine representation, the existence

of the intermittency ring shows that even some of the higher-order two-point statistical turbulence characteristics of the wake can be replicated by porous disks, justifying their use as static wind turbine models.

Appendix A

Validity of calculating the shape parameter for highly intermittent flows

The shape parameter λ^2 is originally a fitting parameter used to fit the probability density functions to a Castaing distribution (Castaing et al. 1990), given by

$$p(\delta u_\tau) = \frac{1}{2\pi\lambda(\tau)} \int_0^\infty \frac{\mathrm{d}(\delta u'_\tau)}{(\delta u'_\tau)^2} \cdots \exp\left[-\frac{\delta u_\tau^2}{2(\delta u'_\tau)^2}\right] \exp\left[-\frac{\ln^2(\delta u_\tau/\delta u_0)}{2\lambda^2(\tau)}\right], \tag{A1}$$

with

$$(\delta u'_0)^2 = \langle \delta u_\tau^2 \rangle \exp\left[-2\lambda^2(\tau)\right]. \tag{A2}$$

However, with the high number of measurement positions used in this work, and for a range of τ, the time consumption and computational costs are high, so λ^2 must be calculated by other means.

The simplified calculation of λ^2 by Eq. 3 rests on several assumptions (Chillà et al. 1996). Of these, the turbulence is assumed to be fully developed. Many of the measurement positions in this work are in shear layers, that is, in regions where the turbulence cannot be assumed to be fully developed. It is therefore necessary to check whether the calculation of λ^2 by Eq. 3 gives a good description of the probability density function of the velocity increments at time scale τ. In particular, this should be investigated for the high intermittency regions.

One way to evaluate the accuracy of Eq. 3 is by comparing the probability density function of δu_τ with Eq. A1 using the λ^2 obtained by Eq. 3. Figure 14 shows the probability density functions for the ND, low TI case, at $x/D = 10$ and $y/D = 1.90$. Except for very small τ, the fit is good. For very small τ, Eq. 3 underestimates the calculated probability density function for large increments. However, for lower values, Eq. 3 performs satisfactorily for the small scales when λ^2 values are lower. This is shown for the centerline at $x/D = 10$ for the low TI ND case shown in Fig. 15. As such, the values of λ^2 should be interpreted carefully for low values of τ at the high intermittency positions in the outermost measurement regions.

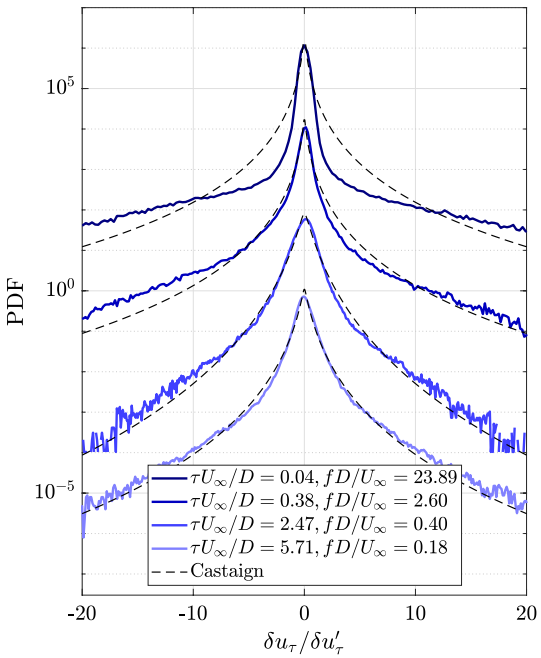

Fig. 14 Probability density function of the velocity increments at $x/D = 10$, $y/D = 1.90$ for the low TI, ND case

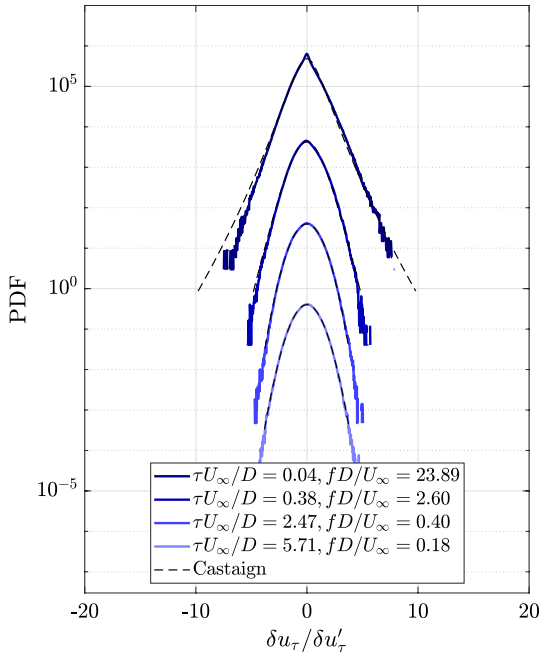

Fig. 15 Probability density function of the velocity increments at $x/D = 10$, $y/D = 0.00$ for the low TI, ND case

Appendix B

Scaled velocity and turbulence intensity profiles

An alternative plotting comparison of profiles of the velocity deficit and TI in the wakes of both disks in both incoming flows are shown in Figs. 16 and 17, respectively.

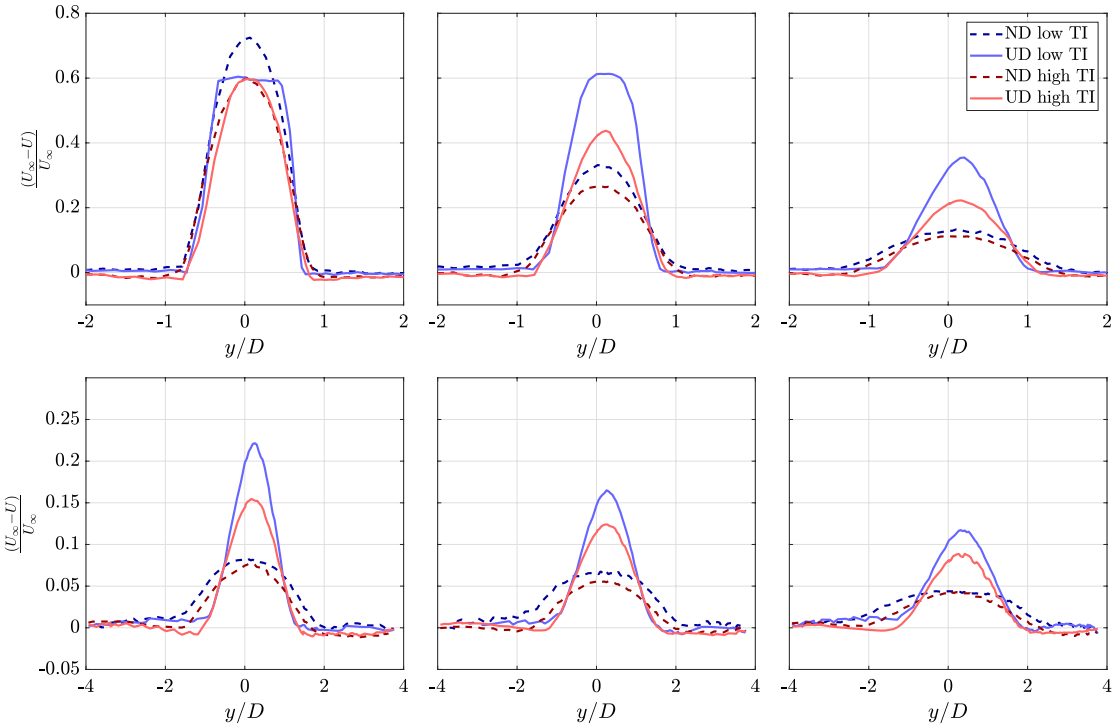

Fig. 16 Profiles of the velocity deficit for all experimental cases, sorted by the streamwise position. Note the different scales between the two rows of figures

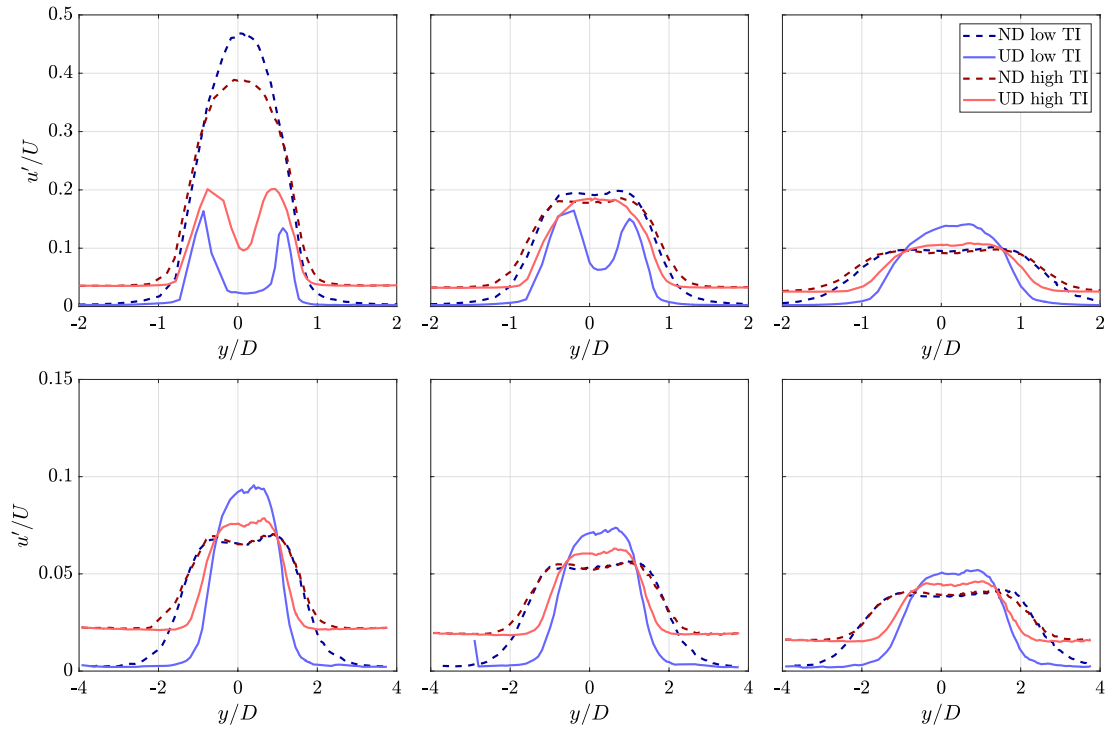

Fig. 17 Profiles of the turbulence intensity for all experimental cases, sorted by the streamwise position. Note the different scales between the two rows of figures

Author Contributions Magnus K. Vinnes, Ingrid Neunaber, Hauk-Morten H. Lykke, and R. Jason Hearst contributed to conceptualization. Magnus K. Vinnes curated data. Magnus K. Vinnes and Hauk-Morten H. Lykke contributed to formal analysis and investigation. Hauk-Morten H. Lykke, Magnus K. Vinnes, and R. Jason Hearst contributed to methodology. R. Jason Hearst administrated the project. R. Jason Hearst contributed to supervision. Magnus K. Vinnes contributed to visualization. Magnus K. Vinnes, Ingrid Neunaber, and Hauk-Morten H. Lykke contributed to writing—original draft. Magnus K. Vinnes, Ingrid Neunaber, R. Jason Hearst, and Hauk-Morten H. Lykke contributed to writing—review and editing.

Funding Open access funding provided by NTNU Norwegian University of Science and Technology (incl St. Olavs Hospital - Trondheim University Hospital). The authors have no funding sources to report.

Data availability statement The data that support the findings of this study are openly available in the NTNU Open Research Data repository at doi: 10.18710/U4JMIV.

Declarations

Ethical approval Not applicable.

Conflict of interest The authors have no competing interests to declare that are relevant to the content of this article.

References

Abdulrahim A, Akpolat MT, Hassanein A et al (2021) Effects of inflow boundary layer on the wake of a radially non-uniform porous disk. J Renew Sustain Energy 13(3):033302. https://doi.org/10.1063/5.0045404

Aubrun S, Loyer S, Hancock P et al (2013) Wind turbine wake properties: comparison between a non-rotating simplified wind turbine model and a rotating model. J Wind Eng Ind Aerodyn 120:1–8. https://doi.org/10.1016/J.JWEIA.2013.06.007 (https://www.sciencedirect.com/science/article/pii/S0167610513001220)

Aubrun S, Bastankhah M, Cal RB et al (2019) Round-robin tests of porous disc models. J Phys: Conf Ser 1256(1):012004. https://doi.org/10.1088/1742-6596/1256/1/012004

Bartl J, Saetran L (2017) Blind test comparison of the performance and wake flow between two in-line wind turbines exposed to different turbulent inflow conditions. Wind Energ Sci 2:55–76. https://doi.org/10.5194/wes-2-55-2017

Bartl J, Mühle F, Schottler J et al (2018) Wind tunnel experiments on wind turbine wakes in yaw: effects of inflow turbulence and shear. Wind Energy Sci 3(1):329–343. https://doi.org/10.5194/WES-3-329-2018

Blackmore T, Batten WM, Muller GU et al (2014) Influence of turbulence on the drag of solid discs and turbine simulators in a water current. Exp Fluids 55(1):1637. https://doi.org/10.1007/S00348-013-1637-9

Bossuyt J, Howland MF, Meneveau C et al (2017) Measurement of unsteady loading and power output variability in a micro wind farm model in a wind tunnel. Exp Fluids 58:1. https://doi.org/10.1007/s00348-016-2278-6

Brown GL, Roshko A (2012) Turbulent shear layers and wakes. J Turbul 13:N51. https://doi.org/10.1080/14685248.2012.723805 (www.tandfonline.com/action/journalInformation?journalCode=tjot20)

Camp EH, Cal RB (2016) Mean kinetic energy transport and event classification in a model wind turbine array versus an array of porous disks: Energy budget and octant analysis. Phys Rev Fluids 1(4):044404. https://doi.org/10.1103/PhysRevFluids.1.044404

Camp EH, Cal RB (2019) Low-dimensional representations and anisotropy of model rotor versus porous disk wind turbine arrays. Phys Rev Fluids 4(2):024610. https://doi.org/10.1103/PhysRevFluids.4.024610

Cannon S, Champagne F, Glezer A (1993) Observations of large-scale structures in wakes behind axisymmetric bodies. Exp Fluids 14:447–450. https://doi.org/10.1007/BF00190199

Castaing B, Gagne Y, Hopfinger EJ (1990) Velocity probability density functions of high Reynolds number turbulence. Physica D 46(2):177–200. https://doi.org/10.1016/0167-2789(90)90035-N

Chillà F, Peinke J, Castaing B (1996) Multiplicative process in turbulent velocity statistics: a simplified analysis. J de Phys II 6(4):455-460. https://doi.org/10.1051/jp2:1996191

Dairay T, Obligado M, Vassilicos JC (2015) Non-equilibrium scaling laws in axisymmetric turbulent wakes. J Fluid Mech 781:166–195. https://doi.org/10.1017/jfm.2015.493

España G, Aubrun S, Loyer S et al (2011) Spatial study of the wake meandering using modelled wind turbines in a wind tunnel. Wind Energy 14(7):923–937. https://doi.org/10.1002/we.515

España G, Aubrun S, Loyer S et al (2012) Wind tunnel study of the wake meandering downstream of a modelled wind turbine as an effect of large scale turbulent eddies. J Wind Eng Ind Aerodyn 101:24–33. https://doi.org/10.1016/j.jweia.2011.10.011 (www.sciencedirect.com/science/article/pii/S0167610511002157)

George WK (1989) The self-preservation of turbulent flows and its relation to initial conditions and coherent structures. In: advances in turbulence. Springer, Berlin

Helvig SdJ, Vinnes MK, Segalini A et al (2021) A comparison of lab-scale free rotating wind turbines and actuator disks. J Wind Eng Ind Aerodyn 209:104485. https://doi.org/10.1016/j.jweia.2020.104485

Higuchi H, Zhang J, Furuya S et al (1998) Immediate and near wake flow patterns behind slotted disks. AIAA J 36(9):1626–1634. https://doi.org/10.2514/2.564

Howland MF, Bossuyt J, Martínez-Tossas LA et al (2016) Wake structure in actuator disk models of wind turbines in yaw under uniform inflow conditions. J Renew Sustain Energy 8(4):043301. https://doi.org/10.1063/1.4955091

Hultmark M, Smits AJ (2010) Temperature corrections for constant temperature and constant current hot-wire anemometers. Measurement Sci Technol 21(10):105404. https://doi.org/10.1088/0957-0233/21/10/105404

Hwang NHC, Baldwin LV (1966) Decay of turbulence in axisymmetric wakes. J Basic Eng 88(1):261–267

Johansson PBV, George WK, Gourlay MJ (2003) Equilibrium similarity, effects of initial conditions and local Reynolds number on the axisymmetric wake. Phys Fluids 15:603. https://doi.org/10.1063/1.1536976

Kankanwadi KS, Buxton OR (2020) Turbulent entrainment into a cylinder wake from a turbulent background. J Fluid Mech 905:A35. https://doi.org/10.1017/JFM.2020.755 (www.cambridge.org/core/journals/journal-of-fluid-mechanics/article/abs/turbulent-entrainment-into-a-cylinder-wake-from-a-turbulent-background/5054CF76C4ED55F8C16BD159A0D94054)

Kolmogorov AN (1962) A refinement of previous hypotheses concerning the local structure of turbulence in a viscous incompressible fluid at high Reynolds number. J Fluid Mech 13(1):82–85. https://doi.org/10.1017/S0022112062000518

Lignarolo LE, Ragni D, Ferreira CJ et al (2016) Experimental comparison of a wind-turbine and of an actuator-disc near wake. J Renew Sustain Energy 8(2):023301. https://doi.org/10.1063/1.4941926

Mi J, Deo RC, Nathan GJ (2005) Fast-convergent iterative scheme for filtering velocity signals and finding Kolmogorov scales. Phys Rev E - Stat Nonlinear Soft Matter Phys. https://doi.org/10.1103/PhysRevE.71.066304

Mi J, Xu M, Du C (2011) Digital filter for hot-wire measurements of small-scale turbulence properties. Measure Sci Technol 22(12):125401. https://doi.org/10.1088/0957-0233/22/12/125401

Morales A, Wächter M, Peinke J et al (2011) Characterization of wind turbulence by higher-order statistics. Wind Energy 15(3):391–406. https://doi.org/10.1002/we.478

Myers LE, Bahaj AS (2010) Experimental analysis of the flow field around horizontal axis tidal turbines by use of scale mesh disk rotor simulators. Ocean Eng 37(2–3):218–227. https://doi.org/10.1016/j.oceaneng.2009.11.004 (www.sciencedirect.com/science/article/pii/S0029801809002613)

Neunaber I, Hölling M, Stevens RJAM et al (2020) Distinct turbulent regions in the wake of a wind turbine and their inflow-dependent locations: the creation of a wake map. Energies 13(20):5392. https://doi.org/10.3390/en13205392

Neunaber I, Hölling M, Whale J et al (2021) Comparison of the turbulence in the wakes of an actuator disc and a model wind turbine by higher order statistics: a wind tunnel study. Renew Energy 179:1650–1662. https://doi.org/10.1016/j.renene.2021.08.002

Obligado M, Dairay T, Vassilicos JC (2016) Nonequilibrium scalings of turbulent wakes. Phys Rev Fluids 1(4):404409. https://doi.org/10.1103/PhysRevFluids.1.044409

Pierella F, Sætran L (2017) Wind tunnel investigation on the effect of the turbine tower on wind turbines wake symmetry. Wind Energy 20(10):1753–1769. https://doi.org/10.1002/we.2120

Pope SB (2000) Turbulent flows. Cambridge University Press. https://doi.org/10.1017/CBO9780511840531

Rind E, Castro IP (2012) Direct numerical simulation of axisymmetric wakes embedded in turbulence. J Fluid Mech 710:482–504. https://doi.org/10.1017/jfm.2012.374

Rind E, Castro IP (2012) On the effects of free-stream turbulence on axisymmetric disc wakes. Exp Fluids 53(2):301–318. https://doi.org/10.1007/s00348-012-1288-2

Schottler J, Bartl J, Mühle F et al (2018) Wind tunnel experiments on wind turbine wakes in yaw: redefining the wake width. Wind Energy Sci 3(1):257–273. https://doi.org/10.5194/WES-3-257-2018

Tennekes H, Lumley J (1972) A first course in turbulence, 1st edn. MIT Press, London

Theunissen R, Worboys R (2019) Near-wake observations behind azimuthally perforated disks with varying hole layout and porosity in smooth airstreams at high Reynolds numbers. J Fluid Eng Trans ASME 141:051108. https://doi.org/10.1115/1.4041614

Theunissen R, Housley P, Allen CB et al (2015) Experimental verification of computational predictions in power generation variation with layout of offshore wind farms. Wind Energy 18(10):1739–1757. https://doi.org/10.1002/we.1788

Toschi F, Amati G, Succi S et al (1999) Intermittency and structure functions in channel flow turbulence. Phys Rev Lett 82(25):5044–5047. https://doi.org/10.1103/PhysRevLett.82.5044

Townsend A (1976) The structure of turbulent shear flow, 2nd edn. Cambridge University Press, Cambridge

Tutkun M, Johansson PBV, George WK (2008) Three-component vectorial proper orthogonal decomposition of axisymmetric wake behind a disk. AIAA J 46(5):1118–1134. https://doi.org/10.2514/1.31074. (**arc.aiaa.org**)

Vinnes MK, Gambuzza S, Ganapathisubramani B et al (2022) The far wake of porous disks and a model wind turbine: similarities and differences assessed by hot-wire anemometry. J Renew Sustain Energy 14:23304. https://doi.org/10.1063/5.0074218

Yu W, Hong VW, Ferreira C et al (2017) Experimental analysis on the dynamic wake of an actuator disc undergoing transient loads. Experiments in Fluids 58:149. https://doi.org/10.1007/s00348-017-2432-9

Yu W, Ferreira C, van Kuik GA (2019) The dynamic wake of an actuator disc undergoing transient load: a numerical and experimental study. Renew Energy 132:1402–1414. https://doi.org/10.1016/J.RENENE.2018.09.013